Polymer Testing 98 (2021) 107186

Contents lists available at ScienceDirect

Polymer Testing

journal homepage: http://www.elsevier.com/locate/polytest

PP/PP-HI/silica nanocomposites for HVDC cable insulation: Are silica clusters beneficial for space charge accumulation?

Xiaozhen He [a], Ilkka Rytöluoto [b], Paolo Seri [c], Rafal Anyszka [a], Amirhossein Mahtabani [a], Hadi Naderiallaf [c], Minna Niittymäki [d], Eetta Saarimäki [b], Christelle Mazel [e], Gabriele Perego [e], Kari Lahti [d], Mika Paajanen [b], Wilma Dierkes [a,*], Anke Blume [a]

[a] University of Twente, Faculty of Engineering Technology, Department of Mechanics of Solids, Surfaces & Systems (MS3), Chair of Elastomer Technology and Engineering, Enschede, the Netherlands
[b] VTT Technical Research Centre of Finland Ltd, Tampere, Finland
[c] University of Bologna, Department of Electrical, Electronic and Information Engineering "Guglielmo Marconi", Bologna, Italy
[d] Tampere University, High Voltage Engineering, Tampere, Finland
[e] Nexans Research Center, 29 Rue Pré Gaudry, 69007, Lyon, France

ARTICLE INFO

Keywords:
HVDC insulation
PP/PP-HI blend
Space charge accumulation
Nanocomposites
Fumed silica

ABSTRACT

New potential High Voltage Direct Current (HVDC) cable insulation materials based on nanocomposites are developed in this study. The nanocomposites are produced by blending of polypropylene (PP), propylene-ethylene copolymer (PP–HI) and a modified fumed silica (A-silica) in a concentration of 1 and 2 wt %. The A-silica is successfully modified with (3-aminopropyl)triethoxysilane (APTES) via a solvent-free method, as proven by infrared spectroscopy, thermogravimetry and transmission electron microscope mapping.

A-silica in the polymer matrix acts as a nucleating agent resulting in an increase of the crystallization temperature of the polymers and a smaller crystal size. Moreover, the silica addition modified the crystals morphology of the unfilled PP/PP-HI blend. The composite containing A-silica with 2 wt% contains bigger-size silica clusters than the composite filled with 1 wt%. The composite with the higher A-silica concentration shows lower space charge accumulation and a lower charge current value. Besides, much deeper traps and lower trap density are observed in the composite with 2 wt% A-silica addition compared to the one with a lower concentration. Surprisingly, the presence of silica clusters with dimensions of more than 200 nm exhibit a positive effect on reducing the space charge accumulation. However, the real cause of this improvement might be due to change of the electron distribution stemming from the amine-amine hydrogen bond formation, or the change of the chain mobility due to the presence of occluded polymer macromolecules constrained inside the high structure silica clusters. Both phenomena may lead to a higher energetic barrier of charge de-trapping, thus increasing the depth of the charge traps.

1. Introduction

The development of the High Voltage Direct Current (HVDC) technology did grow rapidly in the recent decades, owing to its lower cost and lower loss over long distance power transmission than High Voltage Alternating Current (HVAC) technology. This makes the HVDC profitable for integrating it in the remote renewable energy sources network such as wind or solar energy, and for efficiently transmitting electricity to the regions of demand. One of the important elements of the HVDC system is the cable insulation material. In order to further improve the power transmission capacity and increase the voltage of the HVDC transmission, it is crucial to develop new insulation materials for the next generation HVDC cable applications exhibiting low space charge accumulation and electrical conductivity [1–3]. One of the most promising approaches in the insulation material field is the development of dielectric nanocomposites, in which the electrical properties are tuned by addition of selected nano-sized fillers. To characterize the role of a nanofiller in the dielectric nanocomposite, one can consider the following effects:

* Corresponding author.
E-mail address: w.k.dierkes@utwente.nl (W. Dierkes).

https://doi.org/10.1016/j.polymertesting.2021.107186
Received 9 October 2020; Received in revised form 28 February 2021; Accepted 26 March 2021
Available online 30 March 2021

i) Introducing large interfacial areas between their surface and the polymeric matrix: these areas may act as charge scattering centers resulting in an improvement of breakdown strength and voltage endurance [4]. Also, most charge trapping sites are located at the interfacial zone, which has a significant influence on the charge-transport behavior and the space charge accumulation of the nanocomposites [5].
ii) Introducing deep traps: the interface area around the nanofiller show significant charge trapping in nanocomposites. Free-moving charges are trapped by the introduced deep traps in the high electric field and increase the electrostatic barrier reducing further charge injection. Hence, the space charge accumulation is suppressed by addition of the selected nanofillers [6,7].
iii) Modifying the composite morphology with an increase of the loading of a nano-filler like alumina: this way the polymer lamella density increases resulting in a larger interface region, which act as electrical tree propagation channels. Hence, the electrical tree grows like zigzag and becomes bushy, which contributes to slowing down electrical tree propagation. [8];
iv) Tailoring the charge trap distribution: by nanofillers with different surface functionalization the charge trap distribution of the composites can be tailored and thus influence the charge transportation and space charge accumulation. Polyolefin composites containing nanosilica surface-modified with an unpolar silane for example show a higher charge trap density with the same level of trap depth, while nanosilica modified with a polar silane introduces deep charge traps with a low trap density. [9];
v) Increasing the potential barrier for hole tunneling: the addition of common nanofillers with certain band gaps to PE or PP increases the hole tunneling barrier in the amorphous phase of the polymer matrix, and thus leads to the consequent reduction in the conductivity and space charge accumulation [10].

Regarding the base polymer selection driven by sustainability, recyclability of the material is recommended. Due to the crosslinked nature of the state-of-the-art crosslinked polyethylene (XLPE), effective recycling is challenging. Moreover, residues of the crosslinking agent are found to induce space charge accumulation and generally degrade the dielectric properties of the XLPE insulating materials. Therefore, development of a recyclable insulation material becomes indispensable. Polypropylene based materials, which do not need the crosslinking process due to the significantly higher melting temperature compared to PE exhibit a great potential for the next generation insulation application [11,12].

As XLPE and PP, both are unipolar, it is profitable to apply an unpolar nanofiller in order to obtain good compatibility and dispersion [13]. However, in order to introduce deep traps and suppress space charge accumulation [14], some polar functional groups are also beneficial to be grafted on the nanofiller surface. Therefore, finding the right balance between good polymer/filler compatibility and introduction of polar functional groups on the nanofiller surface is a challenge.

In our work, we selected polypropylene/propylene-ethylene copolymer as the insulation polymer blend and a fumed silica modified with polar 3-aminopropyltriethoxysilane as the nanofiller to develop a recyclable dielectric nanocomposite. Besides measuring the composite properties, it was studied whether nanofiller clusters larger than 100 nm can be profitable for the dielectric performance.

2. Materials and experimental methods

2.1. Materials

Fumed silica (Aerosil 200, Evonik, Germany) was selected as nanofiller due to its low water content and branched structure. 3-Aminopropyltriethoxysilane (APTES) was purchased from Sigma Aldrich, The Netherlands. Trifluoroacetic acid used as a catalyst was delivered by Sigma Aldrich, The Netherlands.

The silica modification procedure was as follows: Unmodified silica (20 g) was put into a sealed glass jar and mixed with 3-aminopropyltriethoxysilane (3.6 g) and catalysts, trifluoroacetic acid (0.4 g) and water (0.6 g), at room temperature for 24 h. After the modification, the silica was put in a vacuum oven for another 24 h in order to remove unreacted residuals.

For compounding, polypropylene (PP) (55 wt%) and propylene-ethylene copolymer (PP–HI) (45 wt%) were melt-mixed using a KraussMaffei Berstorff (Germany) ZE25A x 49D UTX twin-screw extruder (cylinder temperature range of 195–230 °C and screw speed 85 rpm) with the surface-modified silica (1 or 2 wt%) and antioxidants (0.3 wt%). The obtained granulated compound was extruded into cast films by a Brabender (Germany) Plasticorder single screw extruder with a T-die and a calendaring system operated at 80 °C. A cast film with a thickness of 300–400 μm was obtained.

2.2. Characterization methods

Silica characterization: Silica samples for FT-IR were prepared with spectroscopic grade KBr, and FT-IR spectra were recorded using a PerkinElmer (USA) Spectrum 100 FT-IR Spectrometer in Diffuse Reflectance Mode (DRIFT). The spectra were recorded at a resolution of 4.0 cm^{-1} and averaged over 128 scans from 4000 to 400 cm^{-1}. The silica samples were also analyzed using thermogravimetric analysis (TGA, TA 550) to quantitatively check the degree of modification. The test was done by heating the sample from 20 °C to 850 °C with a heating rate of 20 °C/min under air atmosphere. The morphology of the silica and elemental mapping were observed by transmission microscopy (Philips, the Netherlands, CM300ST-FEG Transmission Electron Microscope 300 kV).

Composite characterization: Scanning electron microscopy (SEM) was carried out with a Zeiss (Germany) MERLIN HR-SEM. The cast films were broken in liquid nitrogen, and the cross section was used without further treatment for SEM observation. The DSC test was done by cooling down the sample to-50 °C and maintaining it at −50 °C for 5 min, then heating up to 200 °C and maintaining it at 200 °C for another 5 min, followed by cooling down to room temperature with a rate of 3 °C/min under nitrogen atmosphere to mimic the TSDC measurements conditions. Polarized light microscopy (POM, Meiji, Japan, Ml 8530 microscope) was done on the cross section of the microtomed samples with a thickness of 30 μm. X-ray diffraction (XRD, Philips, the Netherlands, X'Pert 1 X-ray diffractometer) were carried on the surface of the compound film. A film was scanned under the 2θ diffraction angle from 5° to 37° (0.05°/8 s). Dynamic mechanical analysis (DMA, Netzsch/Gabo, Germany, Eplexor 2500) was carried out on the compound film by heating the sample from −100 to 140 °C (2 °C/min) with a frequency of 1 Hz (static strain 0.2% and dynamic strain 0.1%).

The polarization current density and thermally stimulated depolarization current (TSDC) were tested on gold-coated compound films. These were firstly coated with gold (10 nm) under high vacuum to serve as the two electrodes. A prepared sample was firstly heated up to 70 °C and stabilized for 3 min, then an electrical field was applied for 20 min. During this process, the polarization current versus time were recorded. The sample was quickly cooled down to −50 °C and stabilized for another 5 min while the voltage was still on. Afterwards, the sample was shorted-circuited for 1 min in order to remove the fast polarization. Finally, the voltage was removed and the sample was linearly heated up to 150 °C with the heating rate of 3 °C/min and the depolarization current versus temperature was recorded. Space charge measurements were done by a pulsed electroacoustic (PEA) test at 60 °C under a DC electric field of 30 kV/mm for 3 h; 1 h depolarization without electrical field was also included.

3. Results and discussion

3.1. Silica characterization

Fig. 1 shows the DRIFT IR spectrums of the reference (Ref.) and APTES modified silicas (A-silica). The broad absorption band around 1222 cm^{-1} for both samples represents the Si–O–Si bond stretching from the silica siloxane main structure. The band at 3747 cm^{-1} originates from the isolated silanol (Si–O–H) groups on the silica surface. It can be used as a measurement of the silica surface modification due to its high reactivity toward silanes [15] and its predominant concentration on the fumed silica surface in comparison to geminal and vicinal silanols. Its concentration reaches 80% of all silanol moieties, measured at a temperature above 400 °C [16]. Before modification, there is an obvious sharp band present at 3747 cm^{-1}, while the band vanishes in the A-silica spectrum. This indicates that APTES reacts with silanol groups on the silica surface, consuming in particular the isolated Si–O–H groups. Furthermore, the bands at 3300 cm^{-1}, 2979 cm^{-1}, 1679 cm^{-1} and 1405 cm^{-1} appear [17] due to the N–H stretching, C–H stretching and N–H bending, respectively, stemming from the APTES silane structure, thus proving that the APTES grafting was successful.

In order to quantitatively investigate the silica surface modification, TGA measurements were done and results are shown in Fig. 2. The A-silica shows a higher weight loss (12,2 wt%) than the Ref. silica (2,7 wt% originating from the loss of the grafted organic groups. This gives further evidence that APTES is grafted on the silica surface successfully. Fig. 3 shows a schematic reaction mechanism of the silane being grafted onto the A-silica surface. The mechanism of the silica modification is based on alkoxy group hydrolysis, which further react with silanol groups on the silica surface. The APTES has three alkoxy groups, which not only react with the silica, but also condense with each other, forming oligomerized structures. Therefore, there is a layer of condensed APTES covering the silica surface, which contributes to the high weight loss of the TGA result.

In order to investigate the morphology of the studied silicas, TEM was performed and results are shown in Fig. 4. The roughness of the silica surface was noticed to be different before and after the modification. In case of the Ref. silica, the surface is smooth and showing primary particles forming a cluster. While the surface of the A-silica is noticeably rougher owing to the modification and the silane oligomerization that covers the silica surface, without visible separation of the primary particles. It is reported in literature that the modification of silica results in a highly nanorough surface [18]. Hence, the change in surface morphology of the silica is another indication of successful APTES grafting onto the silica surface.

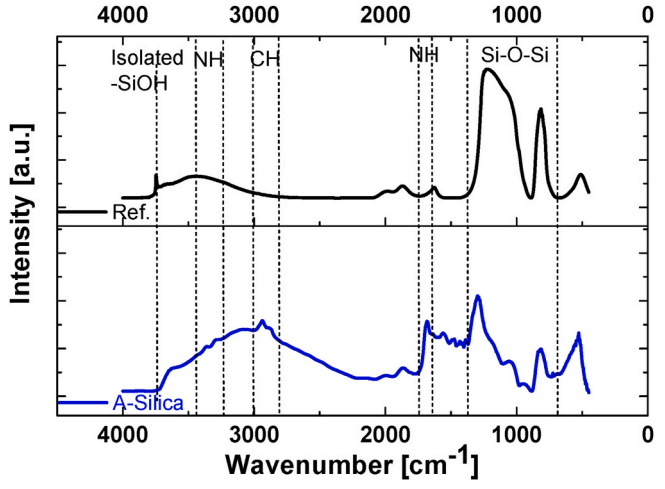

Fig. 1. DRIFT IR spectrum of reference silica (Ref.) and APTES modified silica (A-silica).

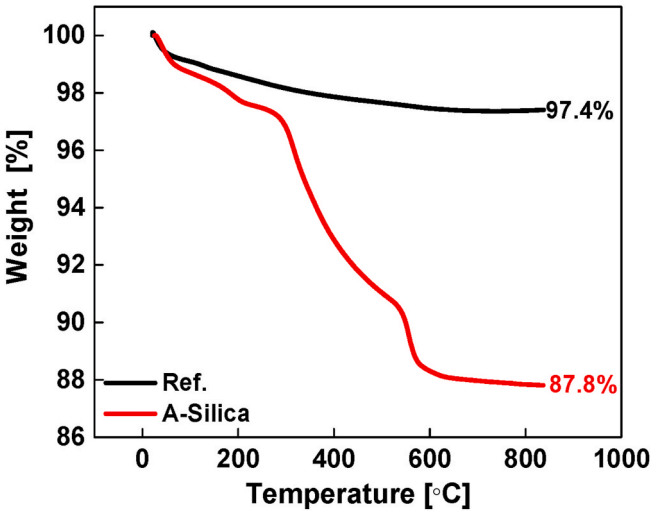

Fig. 2. Mass loss versus temperature of the reference (Ref.) and APTES-modified silica (A-silica).

To further visualize the silica surface modification, HR-TEM elemental mapping was performed, as shown in Fig. 5. The distribution of silicon (A, D) and carbon (B, E) of Ref. and A-silica are shown. For both silica types, a silica-rich area mapping is shown in Fig. 5 (A and D), which is mostly coming from the bulk of the silica and does not show a significant difference between these two samples. However, there is a big difference in the carbon mapping (Fig. 5 B, E): While carbon only vaguely is mapped as shown in the Ref. sample (Fig. 5 B), a carbon-rich area is presented in A-silica (Fig. 5 E), which is stemming from the carbon in the APTES chemical structure. This further proves successful silica modification. Furthermore, in Fig. C and D, the elemental mapping of Ref. barely shows any carbon (in green) on Ref. silica bulk (in red), whereas, the elemental mapping of A-silica (Fig. 5 F) reveals that there is carbon layer (in green) evenly covering the silica (in red) surface. It is also evidenced that the silane distribution is very homogeneous on the A-silica surface.

3.2. Nanocomposites characterization

3.2.1. Morphology and silica dispersion

The polymer blend morphology is considered to be a very important factor for the performance of nanodielectrics. A polymer blend of good compatibility may show a higher electrical breakdown strength and better mechanical properties than the one with low compatibility [19, 20]. The dispersion and distribution of a nanofiller in a polymer matrix are of general concern due to their large effect on the final performance of the nanocomposites. In the field of nanodielectrics, it is agreed that the large interface between a nanofiller and polymeric matrix plays an important role. Hence, the dispersion and distribution of the nanofiller affects the interfacial area and influence the dielectric performance of nanocomposites. Therefore, SEM was performed to study the morphology of the polymer blend and the dispersion of A-silica, as shown in Fig. 6.

There is only one smooth polymer phase present in the unfilled PP/PP-HI blend. It indicates that PP and PP-HI are miscible with each other. This is most likely caused by a high content of polypropylene blocks in the PP-HI, improving its chemical compatibility with PP. Possibly also co-crystallization between the two polymers takes place since they form similar crystallites (Fig. 7). Regarding the dispersion of the silica: agglomerates are present in both nanocomposites. There are three possible reasons for the formation of agglomerates:

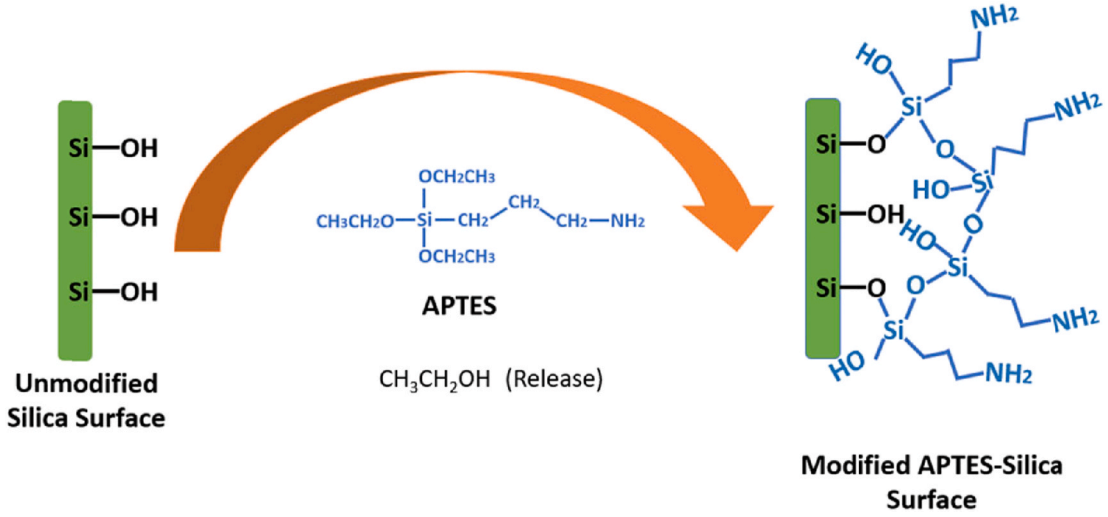

Fig. 3. Schematic diagram of APTES grafting onto the silica surface.

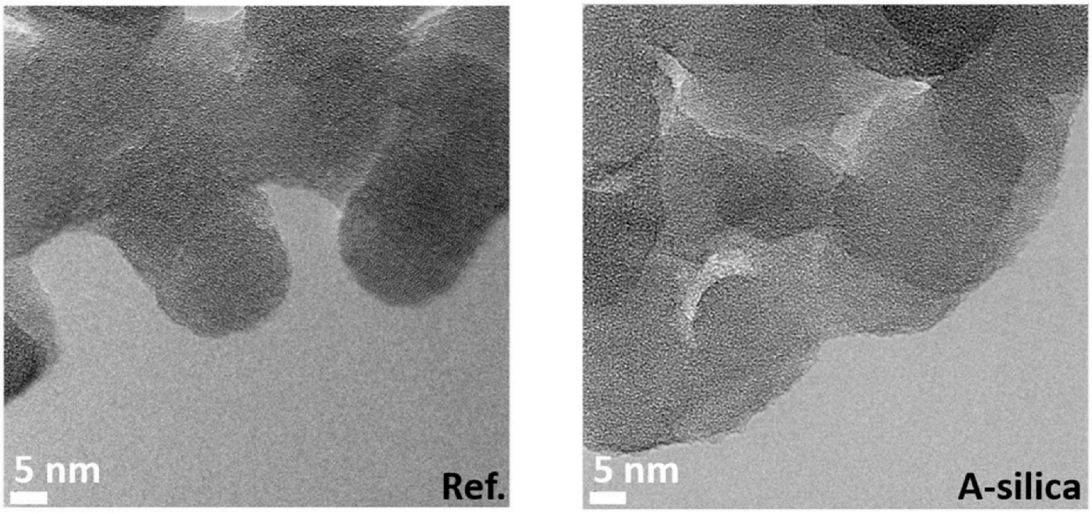

Fig. 4. TEM image of Ref. and A-silica.

1) Due to the high surface area of the silica nanofiller particles, there is a high tendency to reduce their surface energy by forming strong links of physical and chemical nature, which is the driving force to form large agglomerates [21];
2) Hydrogen bond formation through unreacted silanol groups on the silica surface and the amine groups originating from the ATPES grafted onto the silica surface. These hydrogen bonds bind the silica particles together;
3) APTES modified silica still has a polar nature which is not compatible with the unpolar polymeric matrix. Therefore, silica tends to agglomerate together. Moreover, we also notice that the filler dispersion and distribution in the sample with 1 wt % silica is better than when 2 wt% was added. With the increase of the silica concentration to 2 wt %, the average distance between silica particles decreases from 1102 nm (1 wt % silica) to 686 nm (2 wt % silica). Hence, more and bigger agglomerates (200–500 nm) are formed. In comparison, the concentration of 1 wt% of A-silica resulted in a reduced cluster size (30–150 nm), as shown in the histogram in Fig. 6. This can be explained by a higher amount of silica resulting in a higher probability that broken clusters agglomerate during mixing to form bigger clusters.

3.2.2. *Crystallization behavior*

It is reported that the crystallization behavior of semi-crystalline polymers is affected by adding nanofillers [22], and that the changed crystallization behavior can influence electrical insulation properties [23]. Therefore, the crystallization behavior was studied by means of DSC, XRD and POM, as shown in Fig. 7.

In Fig. 7 (a), only one melting peak at around 146 °C for all three samples is visible, which also indicates good miscibility between the PP and PP-HI phases. There is no influence of silica addition on the melting peak as presented in Fig. 7 (a). The crystallization behavior is also shown in Fig. 7 (b). The onset of the crystallization temperature is shifted to higher temperatures by addition of silica regardless of its concentration, which indicates that the silica acts as a nucleating agent, which we observed in earlier work as well [9].

Based on the XRD results as shown in Fig. 7 (c), (the test was done on the surface of the cast film) there are the same type of crystals present in all samples. The main diffraction peaks at $2\Theta = 13.9°$, 16.7°, 18.2°, 20.9°, 21.8° and 25.3° correspond to α(101), α(040), α(130), α(111/040), α(060), respectively. Adding the A-silica does not change the crystal type, as they present the same diffraction peaks with the same location.

Furthermore, crystallinity is decreased by A-silica addition, as

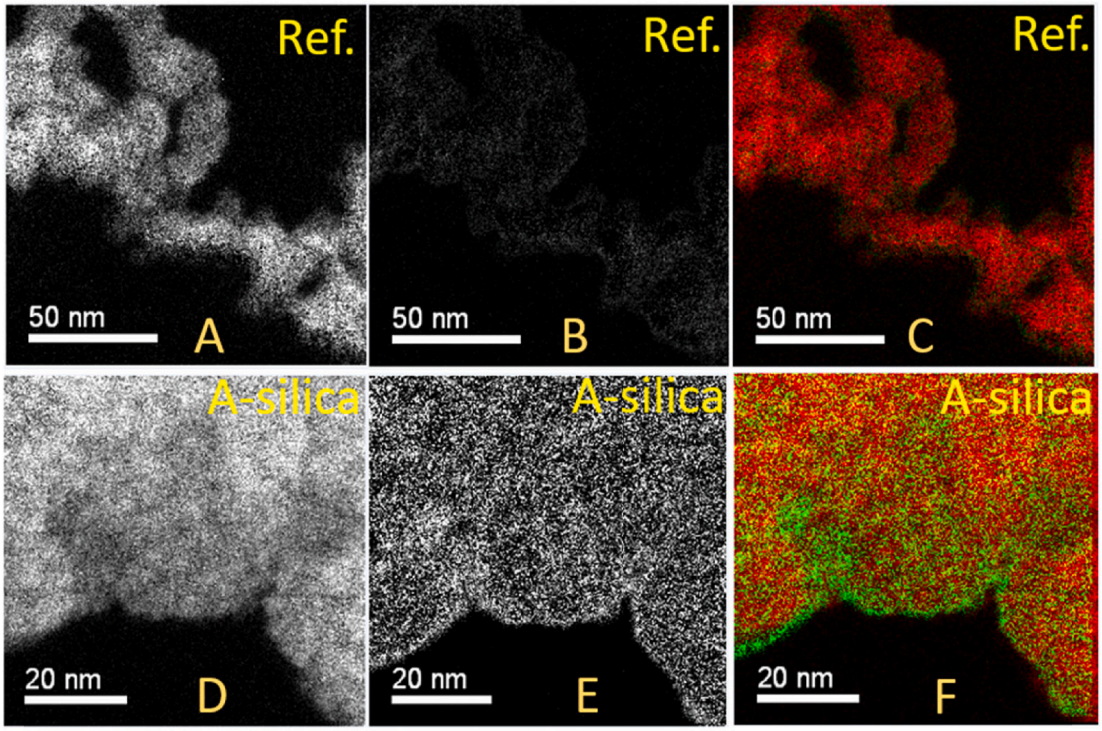

Fig. 5. TEM images and corresponding elemental mapping of Ref. and A-silica.
A,D - silicon mapping; B,E – carbon mapping.C,F - silica elemental mapping (red: silicon; green: carbon).

calculated and shown in Fig. 7 (c). The higher the silica concentration, the smaller the crystalline phase. This is partially evidenced by the XRD results showing a visible decrease of the intensity of the α (040) and α (060) diffraction peaks. Silica is added to the polymer blend in molten state. During cooling, the silica clusters acts as a defect that disturbs the chain ordering process, which results in a lower degree of crystallinity. Compared with 1 wt%, 2 wt % silica addition results in more clusters of larger size, which further block the chain orientation to form crystals. Moreover, the silica acts as nucleating agent, which indicates good interfacial interaction between silica and polymers. During crystallization from the molten state, the immobilized polymer chains located on the silica surface are less likely to crystallize, and thus contribute to lower crystallinity [24]. With 2 wt% silica addition, there is a higher interfacial area between the silica and the polymer blend. Consequently, there are more immobile chains constrained by the silica surface. As a result, adding more silica leads to lower crystallinity. However, this reduction is not linearly correlated with the silica concentration, most likely due to a much more pronounced agglomeration of the silica when its content rises to 2 wt% (Fig. 6). Due to the presence of the bigger clusters, the expected higher silica-polymer interface is relatively reduced, and thus the effect of the crystalline phase decrease is less visible.

Thus the question arises: How is it possible that silica is acting as a nucleating agent, but also decreasing the crystallinity of the polymer? Although the nucleating effect in general contributes to higher crystallinity of the polymer [25], we propose that there are simultaneous effects which lead to decrease of the crystallinity:

1) The process conditions: the cooling gradient (temperature difference over time) upon extrusion of the molten polymer and formation of cast film on the calendaring system, which dictate the effective time for the crystal growth. Therefore, the current process conditions might not be optimal resulting in a short effective time, leading to a less crystals formation;
2) The silica clusters act as structural “defects”, which block the polymer chains arranging during their crystallization;
3) During crystallization in the molten state, the silica surface immobilized polymer chains are less likely to crystallize, and thus do not contribute to crystallinity [24];
4) The increased spherulite disorder with a higher amount of the nucleating agent retards the crystal growth [26];
5) The “competing” effect arising from neighboring nucleation sites for high amount of the nucleating agent might also hinder the crystal formation. More growing spherulites facilitate more intercrystallite interphase hosting the amorphous polymer chains.

To further study the crystallization behavior, POM was performed on microtomed cast film cross sections of unfilled PP/PP-HI blends and PP/PP-HI samples filled with 1% silica or 2% of silica, as shown in Fig. 7 (d), (e) and (f), respectively. A spherulitic crystalline gradient morphology with a mean spherulite size of ca. 5 μm is visible in the unfilled PP/PP-HI sample (Fig. 7 (d)). The spherulite density is higher and the average spherulite size is lower on both the surface layers in comparison to the core region in the unfilled blend, presenting a gradient morphology from the surface towards the inner core of the sample. This effect arises from the processing conditions, most notably the cooling gradient during cast film extrusion, affecting the crystallization process. During the cast film extrusion, as the molten compound exits from the T-die and is extruded on the calendering system chill roll, the cooling rate of the surface layers of the cast film is much higher in comparison to that within the inner core. The temperature gradient from the surface of the sample to the inner core results in spherulitic crystalline gradient morphology.

Interestingly, silica addition significantly changed the crystalline morphology. The nanocomposites do not appear to exhibit gradient type crystalline morphology. Assuming that spherulites are formed, their size in the nanocomposite is too small to be detected and characterized via POM. The formation of small spherulites is due to the nucleating effect of silica, which is in line with the DSC results, as shown in Fig. 7 (b). The amount of the crystalline phase (principally related with the brightness

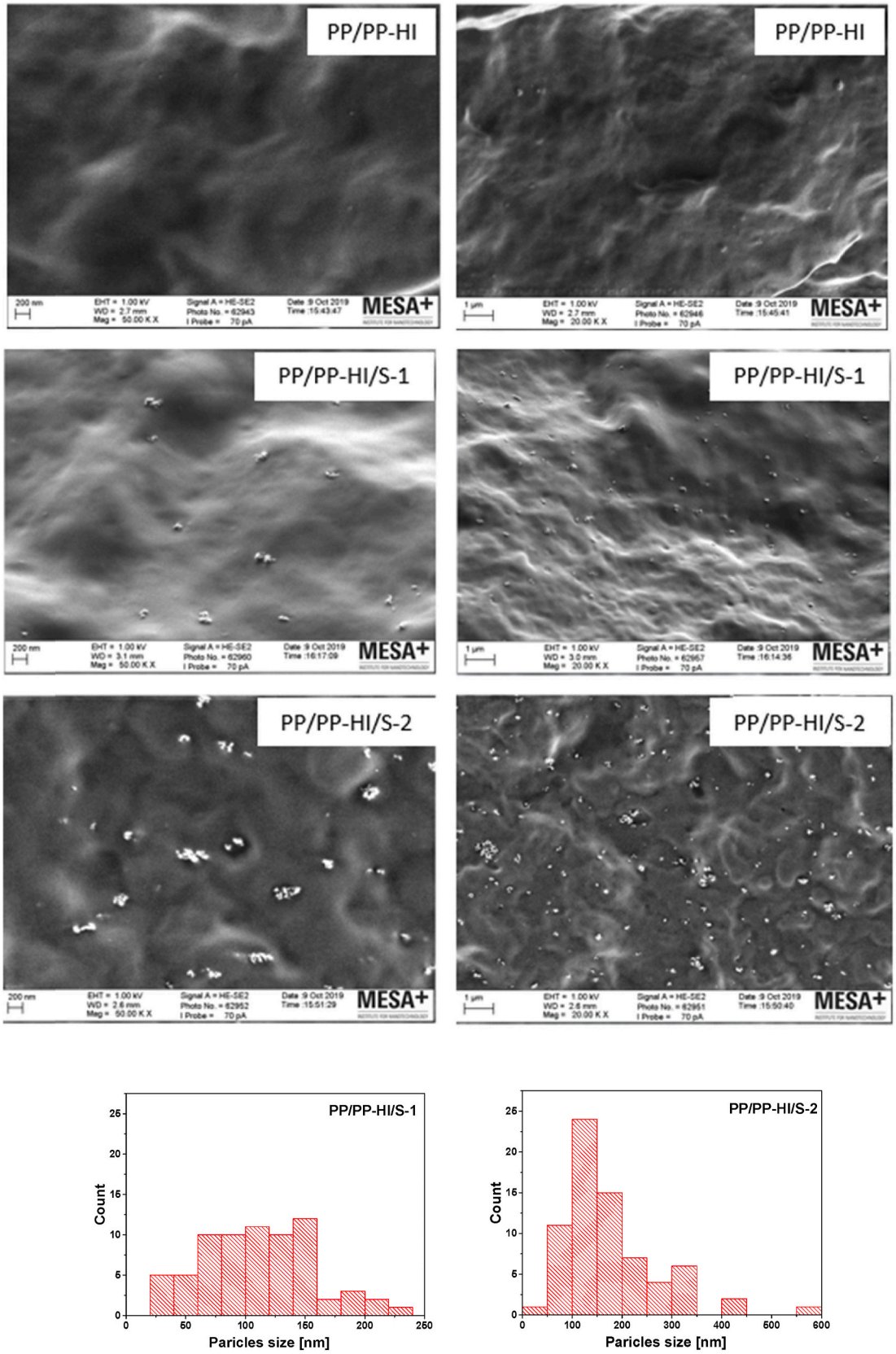

Fig. 6. SEM images of the unfilled PP/PP-HI blend and the nanocomposites filled with 1 wt% (PP/PP-HI/S-1) or 2 wt% of A-silica (PP/PP-HI/S-2) (Left column: 50 k, right column: 20 K). and the histogram of the silica cluster size distribution.

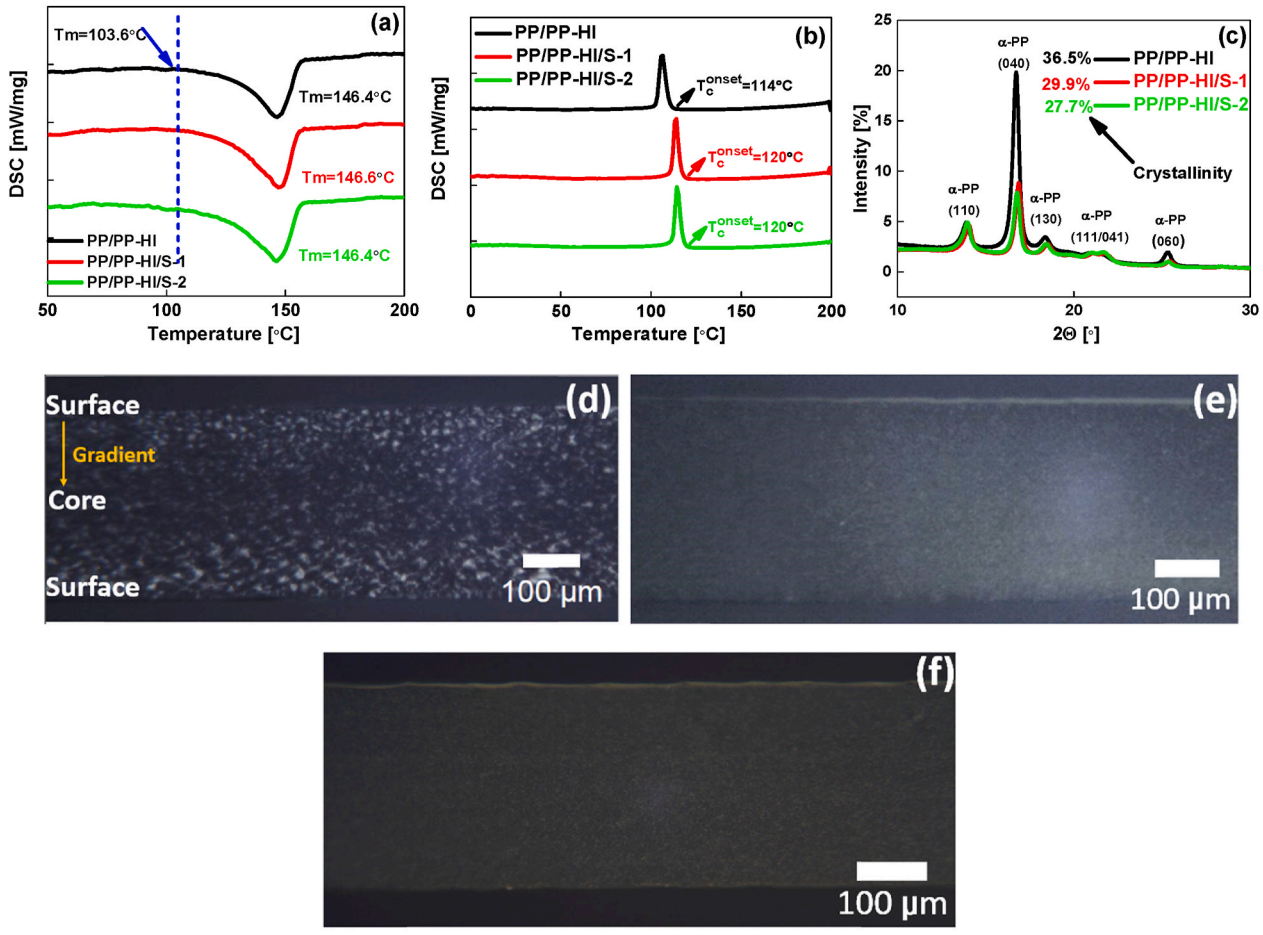

Fig. 7. DSC heating (a) and cooling (b) curves; XRD results of the unfilled PP/PP-HI blend and the nanocomposites filled with 1 wt% or 2 wt% of modified silica (c); POM cross-sectional images of the unfilled PP/PP-HI blend (d); the PP/PP-HI/S-1 (e) and the PP/PP-HI/S-2 (f) nanocomposites.

in the POM images) appears to be lower in the nanocomposites than in the unfilled blend, which is consistent with the XRD results, as shown in Fig. 7 (c).

3.2.3. *Relaxation behavior*

The temperature dependence of the storage modulus, loss modulus and hysteresis (loss factor – tan δ) are presented in Fig. 8. It is a well-known effect that addition of a nanofiller increases the storage modulus of a polymer due to the stiffing effect. The stiffing effect contains two part: 1) the stiff filler and 2) the constrained polymer by the nanofiller forming stiff phase [24], due to the filler polymer interaction. However, in our study, the storage modulus is lower for the silica-filled nanocomposites, and it is much lower in case of 2 wt% silica filled sample compared to the one containing 1 wt%. This is probably due to a dual effect of silica: on one hand, adding silica stiffs the composite, on the other hand, it decreases the crystalline content thus decreases the modulus. Both the effects are competitive to each other; the decrease of the dynamic storage modulus by adding silica is an overlay of both effects. Regarding to the composite containing 2 wt% silica with a relatively low crystallinity compared to the material with 1 wt% silica, the storage modulus decreased more significantly. This might be due to the higher amount and larger silica cluster size. It is likely that the reinforcing potential of the silica is low due to its low amount and its clusters act as local discontinuities which decreases the crystallinity, leading to a lower modulus.

The loss modulus peak represents the glass transition (Tg) of the polymer. There is only one peak in Fig. 8 (b), and it is obvious that the temperature of the glass transition peak does not change by addition of the nanofiller. However, the intensity of the peak is reduced by adding the nanofiller, and addition of 2 wt% of A-silica reduces the peak intensity overproportionally compared to the influence of 1 wt% of A-silica. This might be due to the immobile chains constrained by the nanofiller. It is reported that the "immobilized" matrix associated with the interface between filler and polymer does not contribute to energy loss [27]. Hence, less mobile amorphous chain leads to a reduced β peak intensity. Additionally, the higher amount of A-silica causes relatively more "immobilized" matrix, due to the relatively more constrained rubber chains, leading to a lower amount of the polymer contributing to the energy loss.

Three relaxation peaks (β, α1, α2) correspond to the different transition phases as shown in Fig. 8 (c). The β peak is attributed to the glass transition temperature of the amorphous polymer phase. The α1 peak is related to motions of chain units which lie within the crystalline region of the polymer [28]. The α2 peak is related to melting of the crystalline phase of the polymer. There is no influence of silica addition on the β peak, α1 and α2 peaks.

3.2.4. *Space charge accumulation and charging current density*

Space charge accumulation and conductivity are both major dielectric properties affecting HVDC cable insulation performance under electro-thermal stress. Higher space charge accumulation may lead to accelerated aging and ultimately insulation failure. A higher conductivity of an insulation material would potentially lead to accelerated thermal instabilities and premature breakdown. The influence of nanofillers on these properties are shown in Fig. 9.

In case of the unfilled blend, strong homocharge injection is noticed

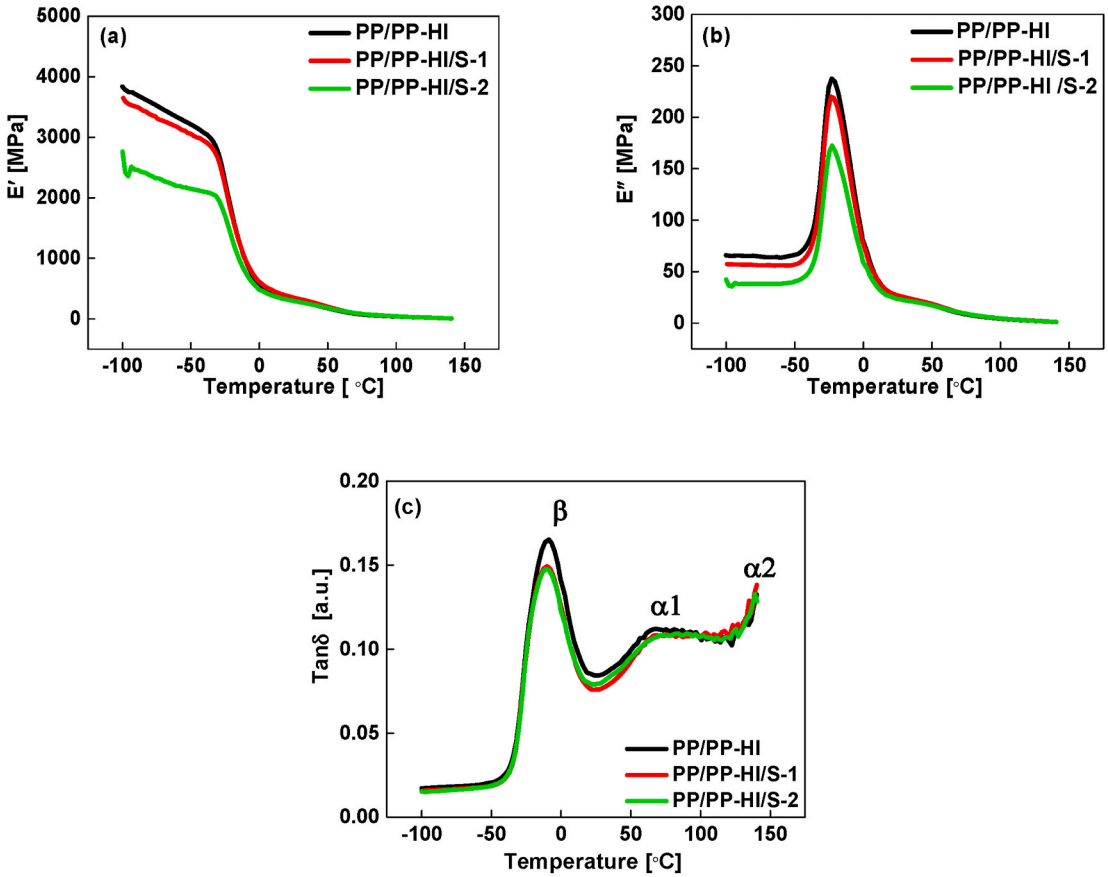

Fig. 8. Storage modulus (a), loss modulus (b) and relaxation behavior (c) temperature dependence of the unfilled PP/PP-HI blend and the nanocomposites filled with 1 wt% or 2 wt% the modified silica.

in the sample, close to the vicinity of both electrodes. This distribution is possibly correlated to the spherulitic crystalline gradient morphology presented in the POM images (Fig. 7 (d)) due to the resulting conductivity gradient present in the bulk of the material. In the surface region of the unfilled blend, the spherulite size is large, which shortens the conduction paths along the inter-spherulite boundaries, and consequently more charges are injected into the unfilled blend. However, in the case of the nanocomposites, the space charge distribution inside the sample is different. A clear negative and positive charge separation can be observed in the vicinity of the cathode and anode, respectively. The mobility of those charge packets is reduced by increasing the concentration of the A-silica. The amount of space charge detected at the end of the polarization period is shown in Table 1. There is a significant amount of space charge (3.0 C/m^3) stored in the unfilled PP/PP-HI blend, while the addition of 1 wt% of A-silica suppresses it to nearly half of that amount (1.6 C/m^3). The addition of 2 wt% of A-silica results in a further significant reduction (0.6 C/m^3).

Depletion of space charge is also different in all three samples. In case of the unfilled PP/PP-HI blend, the charge is drained very quickly, while the A-silica addition reduces this tendency. This indicates that the trap depth in these three samples is different. This result is in line with the trap distribution estimation obtained via TSDC measurements (Fig. 10), in which addition of the silica results in the formation of deeper traps, resulting in slower depletion (relaxation) of trapped charge.

The unfilled blend with the highest initial charging current (during the poling phase of the TSDC measurement) shows a slow polarization behavior with a gradually decreasing current, which results from the superposition of polarization and leakage current (Fig. 9(d)). The initial part of the charging current of the nanocomposites is much lower than the one of the unfilled blend, and they show very fast polarization to reach saturation, which might indicate less space charge formation. This is in line with the PEA results. It is reported that the initial drop can also be explained by the formation of charges in the vicinity of the electrodes due to the presence of nanoparticles, which leads to a higher charge injection barrier, and thus a lower charging current [29]. Furthermore, the current recorded for the PP/PP-HI/S-2 composite is lower than the one for the PP/PP-HI/S-1. Therefore, from the PEA and charging current results during the poling phase, 2 wt% of A-silica gives the best outcome and shows a promising trend for HVDC cable application in terms of the lowest space charge accumulation (under 30 kV/mm) and low current density (under 3 kV/mm).

3.2.5. *Trapping and de-trapping behavior*

In order to gain a better understanding of the space charge and conductivity behavior of the samples, the trap distribution was studied by means of TSDC and the results are shown in Fig. 10. There are two prominent TSDC peaks (P1 and P2) present in the unfilled PP/PP-HI blend. The silica addition suppressed the first peak (P_S-1) compared to the P1 peak in the unfilled blend, and introduced an additional main deep trap (P_S-main) peak and another much deeper (incomplete) peak P_S-2 in place of the P2 of the unfilled blend. Moreover, the TSDC peak intensities are reduced for the nanocomposites compared to the peaks of the unfilled blend. Additionally, the addition of 2 wt% A-silica introduces much deeper traps than 1 wt%. The deeper trap indicates lower charge mobility. This is in line with the PEA results (Fig. 9), in which the charge depletion rate during depolarization is lower for the nanocomposites than for the unfilled blend, and the depletion rate is much slower when 2 wt% A-silica was added compared to 1 wt%.

In the case of the unfilled blend, the first peak is located around 50 °C with the temperature from 25 °C to 100 °C and the second peak is above

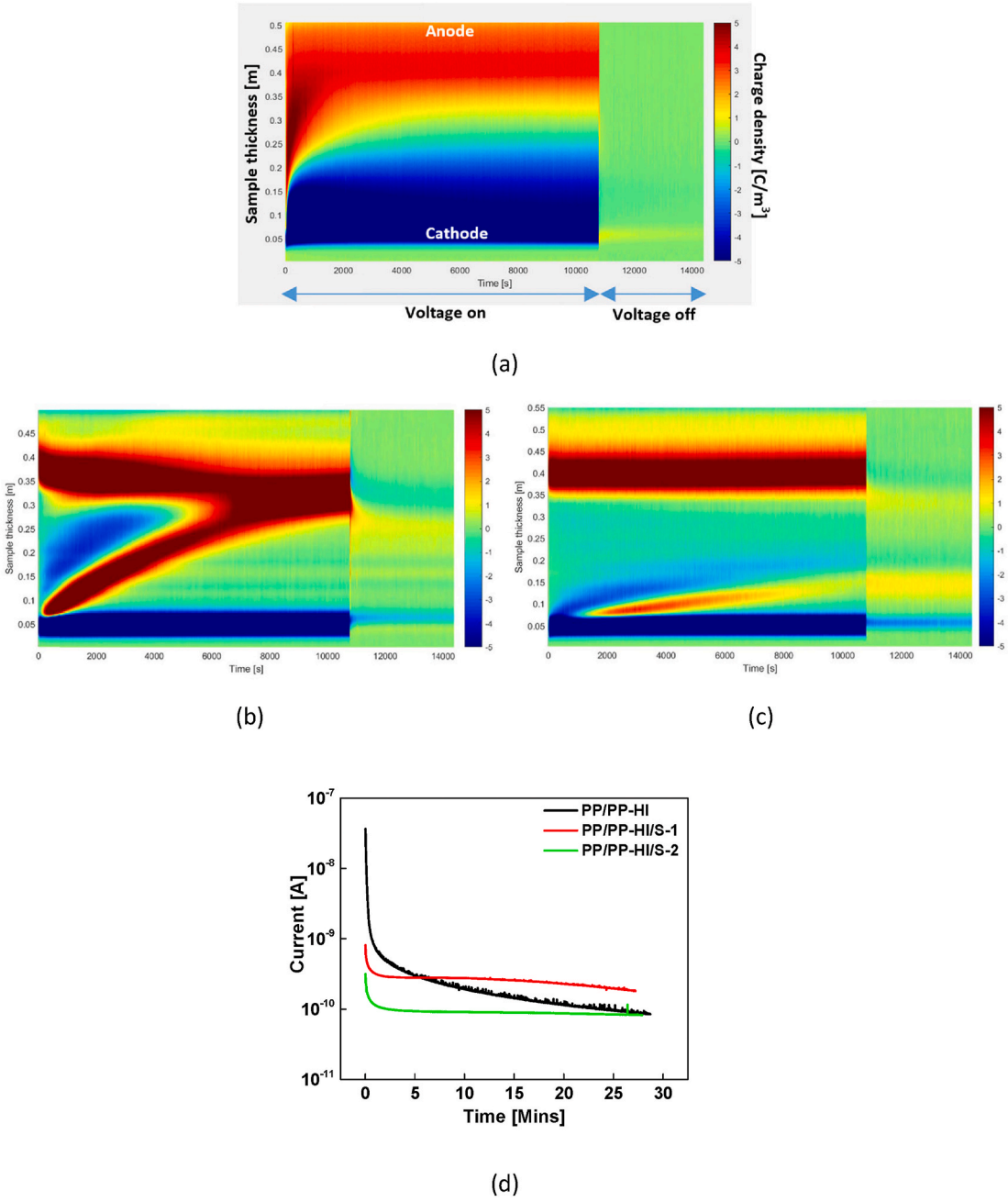

Fig. 9. Space charge profile of unfilled PP/PP-HI blend (a), the nanocomposite filled with 1 wt% A-silica (b) and filled with 2 wt% A-silica (c), current versus time during poling in the TSDC test (d).

Table 1
Amount of space in the samples charge after Volt-off.

Sample	PP/PP-HI	PP/PP-HI/S-1	PP/PP-HI/S-2
Amount of space charge after Volt-off [C/m^3]	3.0	1.6	0.6

100 °C, which is identical with the α1 and α2 relaxation transition peaks (DMA results), respectively, as shown in Fig. 11 (a). It should be stressed that there is a different frequency used for DMA (1 Hz) and TSDC (about 10^{-4} Hz) measurements. Fig. 11 shows the general relationship between the charge de-trapping (TSDC) and molecular relaxations (DMA) observed in corresponding temperature ranges. It is not meant to directly compare the peak temperature positions (related to trap depth) from TSDC with the one observed in the DMA measurements (tan δ). Nevertheless, the coincidence between the P1, P2 peaks from TSDC with the α1 and α2 relaxation transition peaks from DMA reveals that the P1 peak is derived from the charge release related to the chain motions which are restricted in the crystalline phase, and the P2 peak is stemming from the charge released during melting of the crystals. This is line with literature [30]. The above mentioned evidences revealed that the charges are stored at the interface between the amorphous and crystalline phases and within the crystalline structure for the unfilled blend. This also gives an explanation of the PEA pattern (Fig. 9 (a)) of the unfilled blend, which shows the same pattern as the crystal distribution in the POM image (Fig. 7 (d)), which is due to the fact that the charges are trapped around the crystals.

However, for the nanocomposites such an accurate correlation between the TSDC peaks and the chain relaxation peaks in the DMA

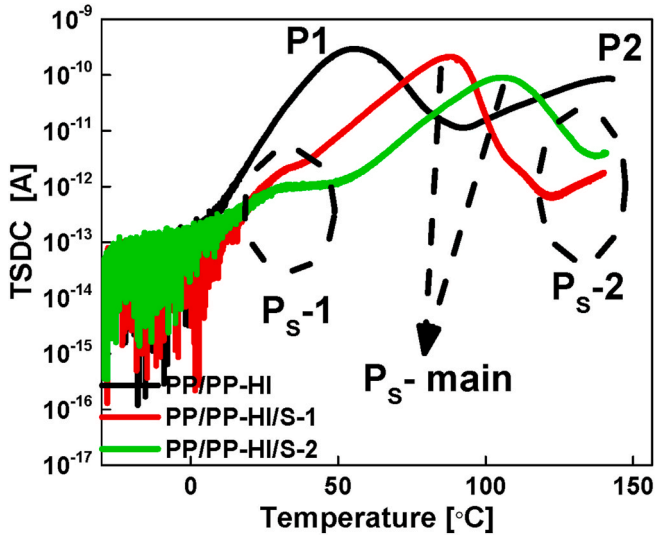

Fig. 10. TSDC curve of the unfilled PP/PP-HI blend and of the nanocomposites filled with 1% (PP/PP-HI/S-1) or 2% A-silica (PP/PP-HI/S-2).

spectra, as shown in Fig. 11 (b, c), cannot be found. Silica addition did not change the α1 and α2 relaxation peaks (Fig. 8 (b)), only changed the TSDC charge release peaks temperature range (Fig. 10). This indicates that the charge location in the nanocomposites might be not be the same as for the unfilled blend. Based on literature, in nanodielectrics the interface between nanofiller and polymeric matrix plays an important role in terms of suppressing space charge accumulation. It was investigated for example that adding ZnO as nanofiller introduces deep traps, which will capture the charge injected from the electrodes, and the trapped charge near the electrodes in turn increases the barrier against charge injection [31]. Therefore, we deduce that most of the charge might be located at the interface between the silica surface and polymer matrix. Hence, the new interface between silica and polymer act as deep traps and suppresses trap density. We observed 3 TSDC peaks (P_S-1, P_S-main, P_S-2) originating from the nanocomposites. In a previous study, we found that the main trap level (P_S-main) is related to the interface between silica and polymer, and that the trap level and trap density depend on the type of surface functionalization (with different chemical moieties) and surface properties [9]. The very small amount of traps type P_S-1 is related to the polymer chain relaxation α1, similarly to P1 from the unfilled blend. Therefore, these traps correspond to the chain motion which are restricted in the crystalline phase. Regarding the deepest traps P_S-2 located at 120 °C and 140 °C for PP/PP-HI/S-1 and PP/PP-HI/S-2, respectively, there are three possible explanations:

1) Melting of the PP/PP-HI blend occurs in the range of 110 °C–160 °C, so the P_S-2 traps are in the range of the polymer melting. Consequently, these traps might still be related to melting of the crystals. However, the P_S-2 traps of the nanocomposites are deeper than the P2 traps of the unfilled blend, which might be a result of the changed crystal size and morphology by addition of the nanosilica, as proven by POM images in Fig. 7 (d, e and f);
2) Since A-silica acts as nucleating agent, it induces crystal grow resulting in possible changes of the interface between the silica and the induced crystalline phase. This might possibly also to contribute to deep trap P_S-2 formation in the nanocomposites;

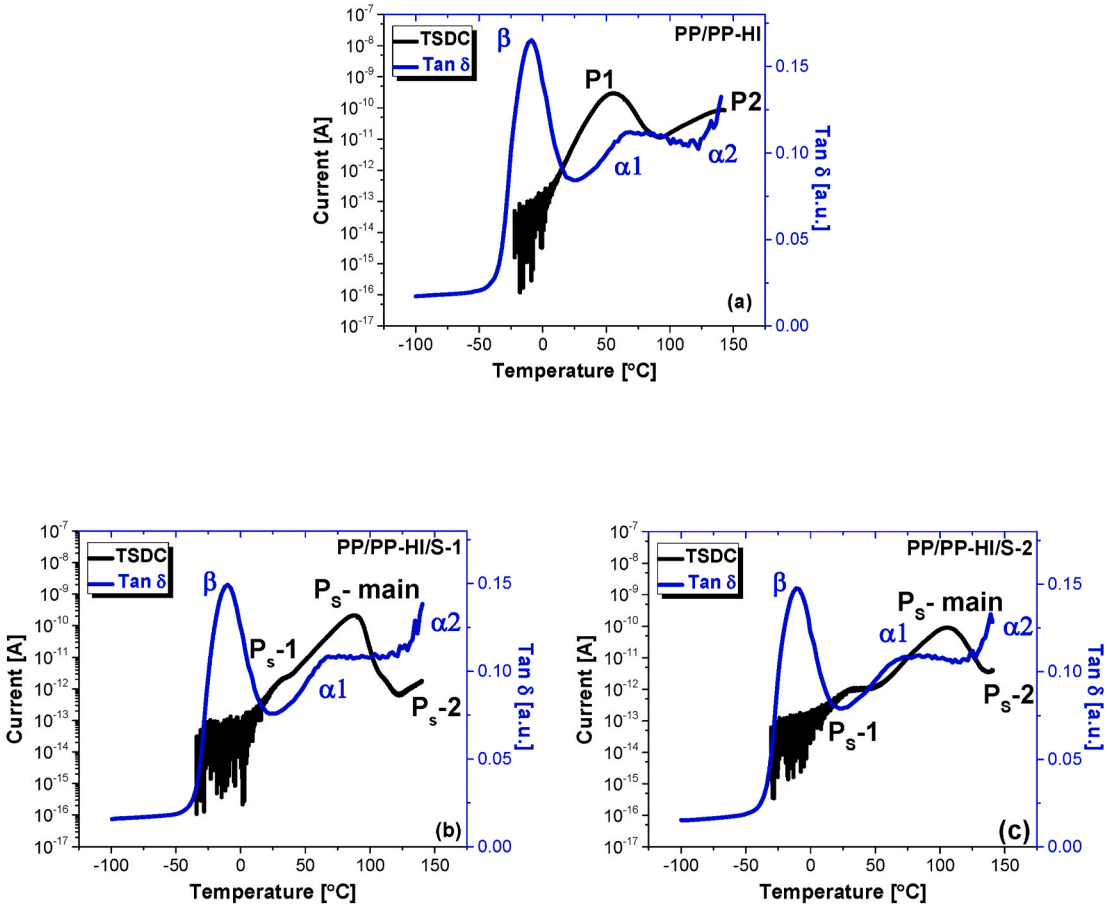

Fig. 11. The relationship between TSDC and DMA relaxation peak of the unfilled PP/PP-HI blend (a) and the nanocomposite filled with 1% (b) or 2% A-silica (c).

3) Based on the literature [32], the deepest traps introduced by silica addition might be directly related to the silica itself. It is stated that since the temperature of the deepest trap release is higher than the melting temperature of the polymer, the silica itself might form the deepest traps in the nanocomposites.

When comparing these three trap levels (P_S-1, P_S-main, P_S-2), the P_S-main peak, which is related to the interface between the silica and polymer, is predominant. This shows, that most of the charges are located in the interface between the A-silica and the polymer matrix.

Consequently, another question is raised. Why does the addition of 1 wt % or 2 wt % of A-silica result in a different main peak level (P_S-main)? The 3-aminopropyltriethoxysilane is located on the A-silica surface, introducing polar amine groups as shown in Fig. 3. The amine moiety has an electrically active dipole nature, which could attract a travelling electron to the silica surface, which might be one of the reasons that the charges are located in the interface between silica and polymer. This could lead to formation of a charge barrier around the silica clusters, which would prevent further charge from injection. As a result, the lower space charge accumulation and lower conductivity are exhibited by the nanocomposites. Furthermore, a higher silica concentration gives a stronger barrier. Consequently, less injected charge results in lower trap density, which also leads to much lower space charge accumulation for the sample with 2 wt% of A-silica compared to the one with 1 wt%.

Furthermore, regarding the dispersion of A-silica (Fig. 6), there are more silica clusters with larger dimensions and higher structures formed in the sample containing 2 wt% A-silica. The deeper Ps-main traps recorded for the PP/PP-HI/S-2 nanocomposite may come from the tightly constrained polymer chains inside of the cluster, as shown in Fig. 12. A tightly constrained polymer chain is less mobile. When the charges are trapped at the interface between the highly constrained polymer and silica, which has a very high energy potential, the charge cannot move or de-trap easily. Furthermore, the immobile trapped charge might form another barrier based on the repelling force suppressing further charge injection, which results in low trap density, low space charge accumulation and also low current density.

Another possibility of the higher trap level with 2% silica addition than 1% might stem from amine-amine hydrogen bonding, as shown in Fig. 13. Based on our previous study [9], nitrogen in amino groups plays an important role for the deep traps in the polymer matrix. Once there are more silica clusters of larger size and higher structure present, more hydrogen bonds are formed between amino groups. As a result, the changed cloud of electrons around nitrogen may induce deeper traps visible in the PP/PP-HI/S-2 peak in comparison to PP/PP-HI/S-1. Furthermore, if charges trapped around one amino group get enough energy to de-trap, it is highly likely that they will be easily trapped by a neighboring amino group. This leads to a lower mobility of the charges.

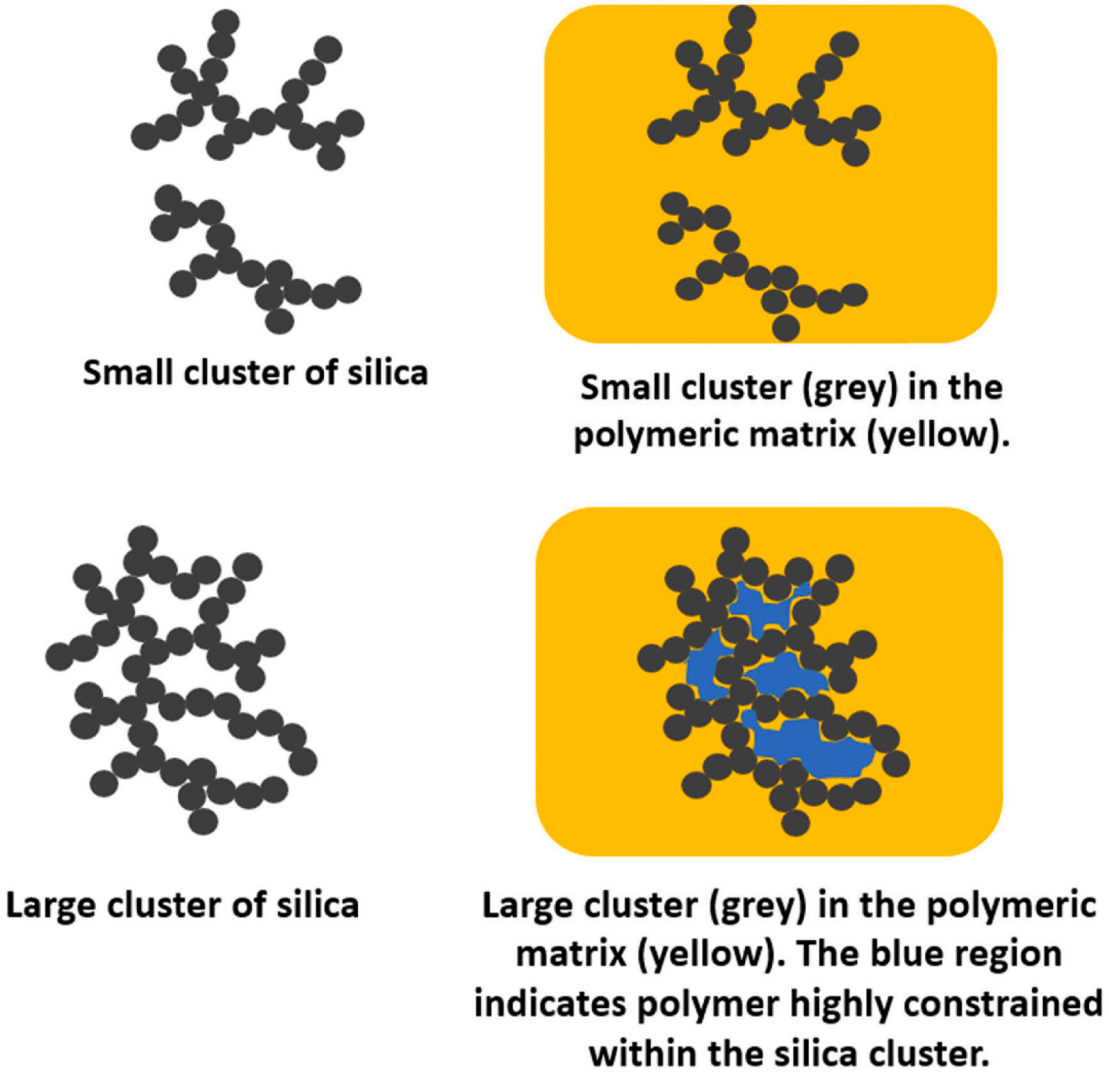

Fig. 12. Schematic diagram of small and large silica clusters and their interaction with polymer macromolecules.

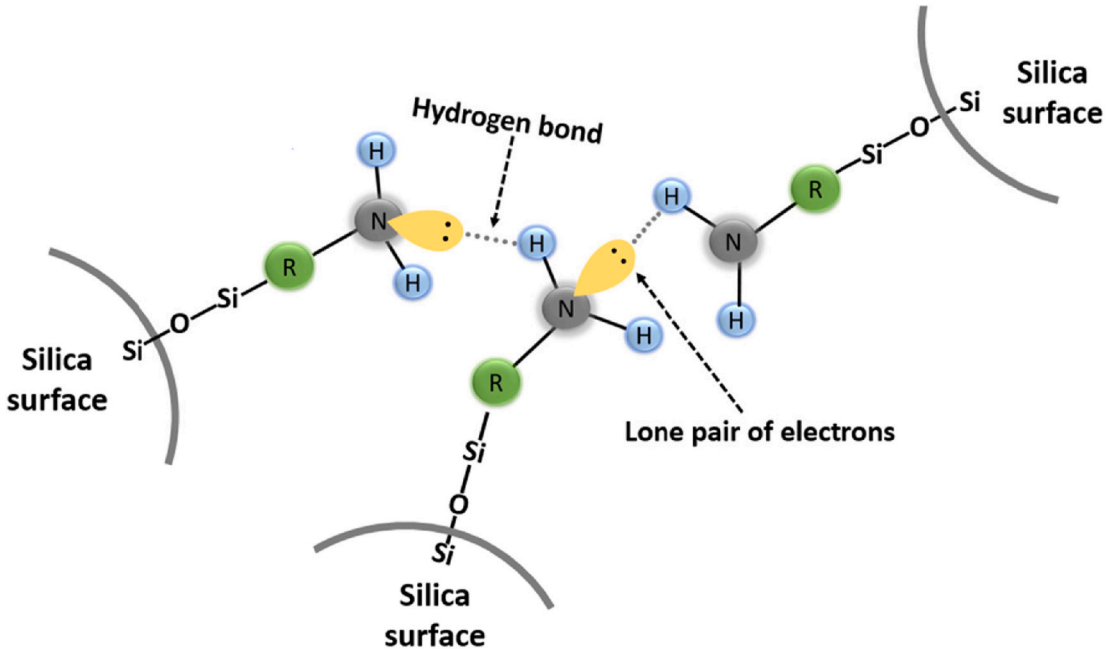

Fig. 13. Schematic diagram of amine-amine hydrogen bond formation inside a silica cluster.

3.3. *In-depth discussion of the dielectric performance*

Based on the POM results in Fig. 7 (d,e,f), there is a pronounced gradient of morphology from the surface towards the inner core region in the unfilled blend, while it does not appear as clearly in the nanocomposites. This is due to the nucleating effect of the nanosilica, resulting in smaller spherulites and their uniform distribution. However, although the nanosilica changed the sample morphology, it did not change the melting temperature of the blend (see DSC results in Fig. 7 (a, b)), consequently no effect on the α1 and α2 chain relaxation is observed in the DMA results in Fig. 8.

In general, morphology as well as presence of additives (e.g. silica) in composites are both able to influence the TSDC charge trapping distribution, hence influencing charge injection, space charge accumulation and conductivity. However, previous work [33] indicates that morphology changes (different spherulite distribution altered by the different compounding techniques) do not significantly change the TSDC charging trap distribution, but they do change the space charge accumulation based on the PEA pattern.

The above observation indicates that the morphology does not influence the values of the TSDC and DMA. But it does influence the charge transportation and space charge accumulation. This is coherent with PEA results.

For an unfilled blend, there is a correlation between the α1 and α2 chain relaxation (DMA results) and the two current peaks from TSDC, as shown in Fig. 11, which gives an indication that most of the charge is located at the amorphous-crystalline interface. The charges may move through the amorphous-crystalline interface at the surface and diffuse to the inner core. However, due to the broader spherulite size distribution observed for the unfilled blend than for the silica-filled composites, the conduction path along the spherulite boundaries is much shorter for the unfilled blend. Hence, in the latter case it is easier to diffuse the charge into the bulk of the unfilled blend. This can be further proven by the PEA pattern (Fig. 9 (a,b,c)): For the unfilled blend, a strong homocharge injection is noticed in the sample, in the vicinity of both electrodes. This distribution can be correlated with the spherulitic crystalline gradient morphology presented in the POM images, and may result in a conductivity gradient in the bulk of the material.

Differently, there is no such correlation in the nanocomposite sample, as the charge trapping near the electrode-polymer interface becomes more pronounced due to increased density of deep traps brought by the nanosilica. This is also related to the crystalline morphology (spherulite size) observed in POM images. It is assumed that most of the charge is located at the filler-polymer interface. Due to the high specific area of the nanosilica, it brings a large interface into the polymer matrix. With the addition of the surface treatment, the amine group on the A-silica surface creates a deep trap at the filler-polymer interface. Additionally, the conduction path along the spherulite boundaries becomes more tedious for the nanocomposites due to the nucleating effect of silica, large specific area of the silica and the surface functionalization. The injected charges can be trapped by the deep traps on the surface region, which can hinder further charge injection to the bulk of the sample. This can be verified by the PEA pattern (Fig. 9 (a,b, c)). The deeper traps reduce charge injection near the electrodes, and less charge can diffuse to the bulk of the sample.

Therefore, all the results can be correlated together to prove that the A-silica changes the morphology of the sample and generates the deep traps into the sample, which changes the charge location and alter the space charge accumulation.

Besides, although 2 wt % of A-silica shows larger size clusters than 1 wt % of A-silica as shown in Fig. 6, the nanocomposite with 2 wt % of A-silica still feature lower space charge accumulation than the one filled with 1 wt % of A-silica: This is due to the much deeper traps introduced by 2 wt % of A-silica. There are two hypothesis to explain the large cluster effect:

1) The deeper charge traps are formed due to the constrained polymer chain in the structure of 2 wt % of A-silica, as shown in Fig. 12. When the charges are trapped at the interface between the highly constrained polymer and silica, which has a very high energy potential, the charge cannot move or de-trap easily, contributing to a deeper apparent trap in the sample filled with 2 wt % of A-silica.
2) The deeper charge traps are formed due to the hydrogen bond formation between amine groups within the silica cluster, as shown in Fig. 13. If charges trapped around one amino group get enough energy to de-trap, it is highly likely that they will be easily trapped by a neighboring amino group. This leads to a lower mobility of the

charges, leading to a deeper apparent trap in the sample filled with 2 wt % of A-silica.

Consequently, a charge trapped in the deeper trap is immobile, which might form another barrier based on the repelling electrostatic force suppressing further charge injection, which finally results in low trap density, low space charge accumulation and also low current density.

4. Conclusions

In this paper, the development of an HVDC insulation material based on PP/PP-HI/A-silica nanocomposites was presented. A-silica was obtained by modifying fumed silica with 3-aminopropyltriethoxysilane (APTES) through a solvent-free silane-silica modification method. The APTES-silica is found to act as nucleating agent, improving the homogeneity crystal distribution in the polymer blend. A-silica addition decreases crystallinity, resulting in a decreased storage modulus. It also introduces deeper traps into the polymeric matrix thanks to the amine groups grafted on its surface. The A-silica addition also changed the charge trapping locations, where for the unfilled blend the charges are mostly located in the crystalline interface and the amorphous-crystalline interface, while for the nanocomposites, charges are mostly located in the A-silica-polymer interface. Although A-silica has a polar nature and is thus not compatible with the polymeric matrix, a higher concentration (2 wt%) of A-silica still benefits the performance of the material by reducing its space charge accumulation and current density. This indicates that the cluster formation with a proper surface functionalization may be beneficial for the dielectric properties in terms of reducing space charge accumulation and apparent conductivity.

CRediT authorship contribution statement

Xiaozhen He: Formal analysis, Investigation, Resources, Writing – original draft, Writing – review & editing, Visualization. **Ilkka Rytöluoto:** Investigation, Writing – review & editing. **Paolo Seri:** Writing – review & editing. **Rafal Anyszka:** Writing – review & editing. **Amirhossein Mahtabani:** Formal analysis. **Hadi Naderiallaf:** Investigation. **Minna Niittymäki:** Investigation. **Eetta Saarimäki:** Investigation. **Christelle Mazel:** Resources. **Gabriele Perego:** Resources. **Kari Lahti:** Writing – review & editing. **Mika Paajanen:** Project administration. **Wilma Dierkes:** Supervision, Writing – review & editing. **Anke Blume:** Supervision.

Declaration of competing interest

The authors declare that they have no known competing financial interests or personal relationships that could have appeared to influence the work reported in this paper.

Acknowledgement

This project has received funding from the European Union's Horizon 2020 research and innovation program under grant agreement ID: 720858.

The authors also would like to thank Evonik Industries for providing a free silica sample.

References

[1] T. Tanaka, T. Imai, Advances in nanodielectric materials over the past 50 years, IEEE Electr. Insul. Mag. 29 (1) (2013) 10–23, https://doi.org/10.1109/MEI.2013.6410535.

[2] J. Thomas, B. Joseph, J.P. Jose, H.J. Maria, P. Main, A. Ali Rahman, B. Francis, Z. Ahmad, S. Thomas, Recent advances in cross-linked polyethylene-based nanocomposites for high voltage engineering applications: a critical review, Ind. Eng. Chem. Res. 58 (46) (2019) 20863–20879.

[3] C. Li, J. Hu, C. Lin, J. He, The control mechanism of surface traps on surface charge behavior in alumina-filled epoxy composites, J. Phys. Appl. Phys. 49 (44) (2016) 445304.

[4] M. Roy, J.K. Nelson, R.K. MacCrone, L.S. Schadler, Candidate mechanisms controlling the electrical characteristics of silica/XLPE nanodielectrics, J. Mater. Sci. 42 (11) (2007) 3789–3799.

[5] Y. Zhou, J. He, J. Hu, B. Dang, Surface-modified MgO nanoparticle enhances the mechanical and direct-current electrical characteristics of polypropylene/polyolefin elastomer nanodielectrics, J. Appl. Polym. Sci. 133 (1) (2016).

[6] B. Han, J. Chang, W. Song, Z. Sun, C. Yin, P. Lv, X. Wang, Study on micro interfacial charge motion of polyethylene nanocomposite based on electrostatic force microscope, Polymers 11 (12) (2019) 2035.

[7] J.W. Zha, Y. Wang, S.J. Wang, M.S. Zheng, X. Bian, Z.M. Dang, Space charge suppression in environment-friendly PP nanocomposites by employing freeze-dried MgO with foam nanostructure for high-voltage power cable insulation, Appl. Phys. Lett. 114 (25) (2019) 252902.

[8] S. Alapati, J.T. Meledath, A. Karmarkar, Effect of morphology on electrical treeing in low density polyethylene nanocomposites, IET Sci. Meas. Technol. 8 (2) (2014) 60–68.

[9] X. He, I. Rytöluoto, R. Anyszka, A. Mahtabani, E. Saarimäki, K. Lahti, M. Paajanen, W. Dierkes, A. Blume, Silica surface-modification for tailoring the charge trapping properties of PP/POE based dielectric nanocomposites for HVDC cable application, IEEE Access 8 (2020) 87719–87734, https://doi.org/10.1109/ACCESS.2020.2992859.

[10] T.J. Lewis, Charge transport in polyethylene nano dielectrics, IEEE Trans. Dielectr. Electr. Insul. 21 (2) (2014) 497–502, https://doi.org/10.1109/TDEI.2013.004173.

[11] Y. Zhou, B. Dang, H. Wang, J. Liu, Q. Li, J. Hu, J. He, Polypropylene-based ternary nanocomposites for recyclable high-voltage direct-current cable insulation, Compos. Sci. Technol. 165 (2018) 168–174.

[12] G.C. Montanari, P. Seri, M. Ritamäki, K. Lahti, I. Rytöluoto, M. Paajanen, Performance of nanoparticles in the electrical behavior of DC capacitor films, in: 2018 12th International Conference on the Properties and Applications of Dielectric Materials, (ICPADM), Xi'an, 2018, pp. 41–44, https://doi.org/10.1109/ICPADM.2018.8401024.

[13] B.N. Rao, V.S. Nandakumar, A study on the dielectric response of polyethylene-metal oxide nanocomposites for electrical insulation in HVDC cables, Mater. Today: Proceedings 18 (2019) 994–1005.

[14] A. Mahtabani, I. Rytöluoto, R. Anyszka, X. He, E. Saarimäki, K. Lahti, M. Paajanen, W. Dierkes, A. Blume, On the silica surface modification and its effect on charge trapping and transport in PP-based dielectric nanocomposites, ACS Applied Polymer Materials 2 (8) (2020) 3148–3160.

[15] B. McCool, L. Murphy, C.P. Tripp, A simple FTIR technique for estimating the surface area of silica powders and films, J. Colloid Interface Sci. 295 (1) (2006) 294–298.

[16] L.T. Zhuravlev, The surface chemistry of amorphous silica, Zhuravlev model. Colloids and Surfaces A: Physicochemical and Engineering Aspects 173 (1–3) (2000) 1–38.

[17] W.C. Wilfong, C.S. Srikanth, S.S. Chuang, In situ ATR and DRIFTS studies of the nature of adsorbed CO2 on tetraethylenepentamine films, ACS Appl. Mater. Interfaces 6 (16) (2014) 13617–13626.

[18] S. Rezaei, I. Manoucheri, R. Moradian, B. Pourabbas, One-step chemical vapor deposition and modification of silica nanoparticles at the lowest possible temperature and superhydrophobic surface fabrication, Chem. Eng. J. 252 (2014) 11–16.

[19] Y. Gao, J. Li, Y. Yuan, S. Huang, B. Du, Trap distribution and dielectric breakdown of isotactic polypropylene/propylene based elastomer with improved flexibility for DC cable insulation, IEEE Access 6 (2018) 58645–58661.

[20] Paolo Seri, Electrical properties of nanostructured polypropylene: a matter of morphology? JICABLE (2019) https://doi.org/10.6092/unibo/amsacta/6304.

[21] S. Fakirov, Polymer nanocomposites: why their mechanical performance does not justify the expectation and a possible solution to the problem? Express Polym. Lett. 14 (5) (2020) 436–466.

[22] S.M. Davachi, B.S. Heidari, R. Sahraeian, A. Abbaspourrad, The effect of nanoperlite and its silane treatment on the crystallinity, rheological, optical, and surface properties of polypropylene/nanoperlite nanocomposite films, Compos. B Eng. 175 (2019) 107088.

[23] J. Yang, M. Gao, H. Zhao, S. Liu, M. Hu, S. Xie, Space charge characteristics of polypropylene modified by rare earth nucleating agent for β crystallization, Materials 12 (1) (2019) 42.

[24] D. Pedrazzoli, A. Pegoretti, K. Kalaitzidou, Interfacial interactions in silica-reinforced polypropylene nanocomposites and their impact on the mechanical properties, Polym. Compos. 37 (7) (2016) 2018–2026.

[25] J.H. Liu, J.H. Cai, X.H. Tang, Y.X. Weng, M. Wang, Achieving highly crystalline rate and crystallinity in Poly (l-lactide) via in-situ melting reaction with diisocyanate and benzohydrazine to form nucleating agents, Polym. Test. 81 (2020) 106216.

[26] S. Alapati, J.T. Meledath, A. Karmarkar, Effect of morphology on electrical treeing in low density polyethylene nanocomposites, IET Sci. Meas. Technol. 8 (2) (2014) 60–68.

[27] M. Sumita, H. Tsukihi, K. Miyasaka, K. Ishikawa, Dynamic mechanical properties of polypropylene composites filled with ultrafine particles, J. Appl. Polym. Sci. 29 (5) (1984) 1523–1530, https://doi.org/10.1002/app.1984.070290506.

[28] E. Laredo, N. Suarez, A. Bello, B.R. de Gáscue, M.A. Gomez, J.M.G. Fatou, α, β and γ relaxations of functionalized HD polyethylene: a TSDC and a mechanical study, Polymer 40 (23) (1999) 6405–6416.

[29] L.K.H. Pallon, A.T. Hoang, A.M. Pourrahimi, M.S. Hedenqvist, F. Nilsson, S. Gubanski, U.W. Gedde, R.T. Olsson, The impact of MgO nanoparticle interface in ultra-insulating polyethylene nanocomposites for high voltage DC cables, J. Mater. Chem. 4 (22) (2016) 8590–8601, https://doi.org/10.1039/c6ta02041k.
[30] T. Mizutani, Y. Suzuoki, M. Ieda, Thermally stimulated currents in polyethylene and ethylene–vinyl-acetate copolymers, J. Appl. Phys. 48 (6) (1977) 2408–2413.
[31] B. Dang, Q. Li, Y. Zhou, J. Hu, J. He, Suppression of elevated temperature space charge accumulation in polypropylene/elastomer blends by deep traps induced by surface-modified ZnO nanoparticles, Compos. Sci. Technol. 153 (2017) 103–110.
[32] M. Gao, J. Yang, H. Zhao, H. He, M. Hu, S. Xie, Preparation methods of polypropylene/nano-silica/styrene-ethylene-butylene-styrene composite and its effect on electrical properties, Polymers 11 (5) (2019) 797.
[33] Rytöluoto, I., Saarimäki, E., Pelto, J., Paajanen, M., He, X., Anyszka, R., Mahtabani, A., Dierkes, W., Seri, P., Naderiallaf, H. and Lahti, K., Feasibility of Mini-Scale Injection Molding for Resource-Efficient Screening of PP-Based Cable Insulation Nanocomposites.